JOURNAL OF GEOPHYSICAL RESEARCH, VOL. 103, NO. D20, PAGES 25,975–25,995, OCTOBER 27, 1998

A general circulation model study on the interannual variability of soil dust aerosol

Ina Tegen[1] and Ron Miller[1]

Department of Applied Physics, Columbia University, New York

Abstract. To assess interannual soil dust aerosol variability, we computed dust as a tracer in the Goddard Institute for Space Studies general circulation model. Comparisons of dust model results with results from an off-line tracer model, satellite retrievals, and ground observations show mostly good agreement, but also reveal problems with the model results and difficulties with such comparisons. Two 15–year runs with prescribed sea surface temperatures were carried out, one with identical dust sources for each year and one with varying dust sources in order to investigate the contribution of dust sources and transport to the variability of dust concentrations in different regions. Specifically for the North Atlantic and the Mediterranean region, 70-90% of the dust variability is attributable to transport variability. Correlation coefficients between dust concentrations with precipitation and surface winds were calculated to find controlling factors for dust concentration for different regions of the world.

1. Introduction

Because of its high atmospheric mass load, soil dust aerosols are not only a potentially important climate forcing factor, but may also impact atmospheric chemistry by providing surfaces for heterogeneous chemical reactions [*Dentener et al.,* 1996]. Interannual variations in the atmospheric dust load can be caused by changes in meteorological factors (like surface wind speed and rainfall) or by changes in land surface conditions. Several previous studies described off-line transport model results of the soil dust cycle [*Wefers and Jaenicke,* 1990; *Tegen and Fung,* 1995; *Marticorena and Bergametti,* 1996]. Such studies are well-suited to test source and sink parameterization of soil dust, but cannot address dynamic feedback mechanisms. Other studies included soil dust as a tracer in a full general circulation model (GCM) [*Joussaume,* 1990; *Genthon,* 1992] mainly for the purpose of simulating dust distributions under paleoclimate conditions; those studies did not include the radiative impact of dust. Very few studies addressed the radiative impact of dust on GCM dynamics [*Coakley and Cess,* 1985; *Miller and Tegen,* 1998], but those studies used a prescribed dust distribution that could not be modified by perturbations to circulation forced by dust.

As a first step toward the calculation of the effects of radiatively interactive dust in a GCM, we included dust as a dynamic tracer in the Goddard Institute for Space Studies (GISS) atmospheric GCM to assess the relationship between dust production and transport and climate modes. Specifically, we investigate how the dust production in the model is correlated with climate parameters like precipitation and surface winds. For the studies described here, the dust does not interact with radiation, and fixed climatological sea surface temperatures (SSTs) are used as a lower boundary condition. The purpose of this study is not to obtain a highly realistic dust distribution (for this purpose, the GCM resolution is too coarse) but rather to obtain information about the sensitivity and variability in dust production and transport, which are described in this paper. Another goal of this study is to determine regions where the primary cause of variability in dust concentrations is the variability of source strength rather than transport variations. In those regions we can expect that observed changes in dust concentrations are caused by changes in source strengths resulting from, for example, anthropogenic changes in soil surface conditions.

2. Dust Parameterization in the GISS GCM

Dust was included as an interactive tracer in the GISS GCM using GCM-predicted values of wind speed and precipitation to calculate dust sources, transport, and deposition. An updated version of the model described by *Hansen et al.* [1983] was used, with a new convection/cloud scheme and ground hydrology parameterization [*DelGenio et al.,* 1996; *Hansen et al.,* 1997]. In

[1]Also at NASA Goddard Institute for Space Studies, New York.

Paper number 98JD02345.
0148-0227/98/98JD-02345$09.00

these experiments the boundary layer parameterization of *Zinn and Kowalski* [1995] was used. The parameterization of dust as a tracer in the GISS GCM follows the calculation of dust in the off-line GISS tracer transport model [*Tegen and Fung,* 1994]. We first review the parameterization of dust in these previous studies, before describing the dust parameterization in the GCM. In the off-line calculations (the former study), dust fluxes were computed using European Centre for Medium Range Weather Forecast (ECMWF) surface-wind products with a spatial resolution of 1.125° × 1.125° and a 6-hour time step. Dust emissions were also dependent on soil moisture, vegetation cover, and soil surface conditions. Transport above the surface in the off-line tracer model was calculated using wind fields and subgrid-scale mixing that was extracted from the 4° × 5° version of the GISS GCM. Dust distributions were calculated for eight size classes, as the radiative properties of dust are strongly dependent on particle size distribution [*Lacis and Mishchenko,* 1995], which changes during transport as larger particles settle more quickly.

In the present new study, GCM dust emission was similarly computed as a function of surface conditions (vegetation cover and land use), surface wind speed, and soil moisture. The surface wind speed was predicted hourly by the GCM instead of the ECMWF values used in the off-line model. The GCM transported four size classes of dust as independent tracers with size ranges of 0.1-1, 1-2, 2-4, and 4-8 μm. The number of size classes is smaller compared to the off-line tracer model but was sufficient for this computation. Sizes below 1 μm were transported as one size class (in contrast to four submicron size classes in the previous study) as they are not strongly fractionated by gravitational settling. Particles larger than 8 μm are only responsible for about 1% of the dust radiative forcing [*Tegen et al.,* 1996] and were neglected. Surface distributions of clay (particles smaller than 1 μm) and small silt (particle radius between 1 and 10 μm) were derived from a global soil texture data set [*Zobler,* 1986; *Webb et al.,* 1991]. The GISS GCM was integrated with a horizontal resolution of 4° × 5° and nine vertical layers (seven tropospheric and two stratospheric layers) as described by *Hansen et al.* [1983]. The dust sources, transport, and deposition were computed with a 1-hour time step.

As described by *Tegen and Fung* [1995], dust deflation (i.e., lofting of dust from soil surfaces) is allowed in areas that are labeled by *Matthews* [1983] as deserts or sparsely vegetated regions, as well as from disturbed soils which are affected by deforestation, cultivation in dry regions, wind erosion, and the shift in the Saharan/Sahelian boundary [*Middelton,* 1992; *World Resources Institute,* 1992; *Tucker et al.,* 1991]. Dust deflation can only occur for low soil moisture conditions. Instead of using a condition for soil matrix potential as described by *Tegen and Fung* [1994], we allowed dust deflation to occur if at a given grid box evaporation had been higher than precipitation for a time period depending on the soil texture. Those time periods were chosen to be 20 hours for sandy ("coarse texture") soils, 50 hours for silty ("medium texture"), and 250 hours for clay ("fine texture") soils. Those values take into account the different diffusivity for different soil types at the same volumetric water content [*Gardner,* 1983], and were chosen to give a realistic extent of source areas. This dependence of source area on precipitation allows for a study of the effect of year-to-year precipitation changes on dust fluxes. Soil condition parameters were calculated in 1° × 1° resolution and then averaged to 4° × 5° degree resolution. Examples for the source extent in the GCM for January, April, July, and October are shown in Figures 1a-1d, respectively. The values shown in Figure 1 are the fraction of particles with radii less than 10 μm [*Webb et al.,* 1991] (which is the radiatively active fraction of soil dust aerosol) in the top 30 cm of the soil, multiplied by the fraction of the grid box designated as a source area and the fraction of hours per month when the grid box can act as dust source, that is, when the soil surface is "dry". Source areas like the Sahara, Gobi Desert, parts of North America, and Australia are reproduced by the model.

Surface wind speed is the most critical factor in the calculation of dust emissions. In the model the amount of uplifted dust in those areas where the surface conditions allow dust deflation follows *Gillette* [1978],

$$q_a = C(u - u_{tr})u^2 \qquad (1)$$

where q_a is the dust flux from the surface in $\mu g\ m^{-2}\ s^{-1}$, u is the surface wind speed in $m\ s^{-1}$, and u_{tr} is a threshold velocity. As described below, different values will be assigned to u_{tr} for each grid box. For wind speeds below this threshold no dust deflation takes place. In the earlier study by *Tegen and Fung* [1995], different values for the dimensional constant C were chosen for undisturbed desert soils and soils that were disturbed by human activities or shifts in climate conditions. This took into account that recently disrupted soil surfaces can contain a higher fraction of fine soil particles available to wind erosion, while in undisturbed soils the fine material is often depleted [*d'Almeida and Schütz,* 1983]. In contrast, here we used the same dimensional constant of C = 2 $\mu g\ s^2\ m^{-5}$ for clay particles (< 1 μm) and C = 5 $\mu g\ s^2\ m^{-5}$ for silt particles (1-8 μm) to describe dust deflation for both disturbed and undisturbed soils, which may lead to an overestimate for the relative contribution of desert soils which are expected to be less effective dust emitters compared to disturbed soils.

When using a uniform surface wind speed threshold, dust fluxes calculated using GCM surface wind speeds with 4° × 5° spatial resolution are considerably different from the dust fluxes calculated with the surface wind products from ECMWF which have higher (1.125° × 1.125°) spatial resolution. The difference in fluxes may be due to the lower spatial resolution or problems in the parameterization of the planetary boundary layer in the GISS GCM. Figure 2 shows a histogram of surface wind speed for a grid box in the Saharan region (15°E, 25°N) derived from the annual

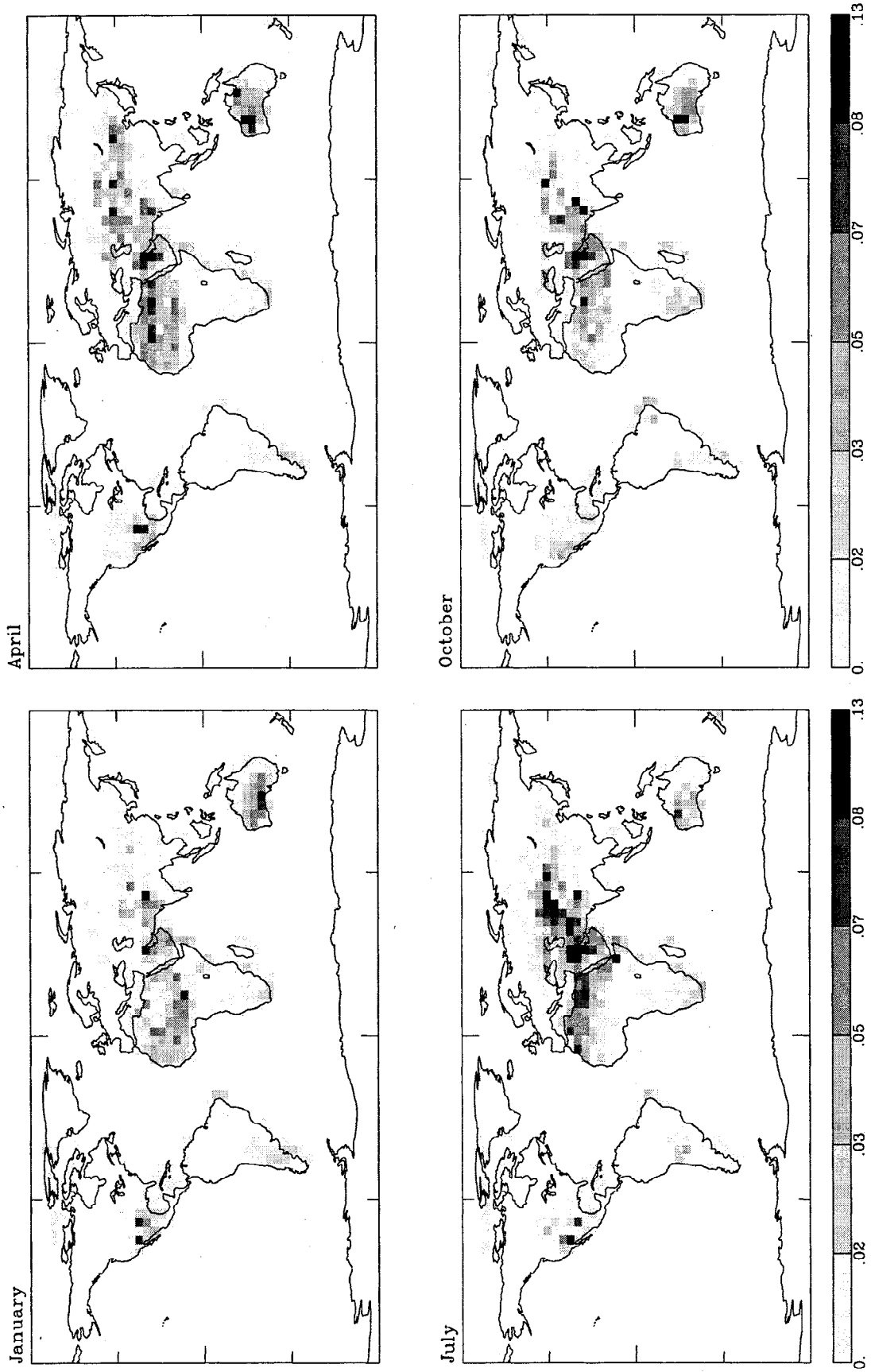

Figure 1. Source areas in the GISS model for the months (a) January, (b) April, (c) July, and (d) October.

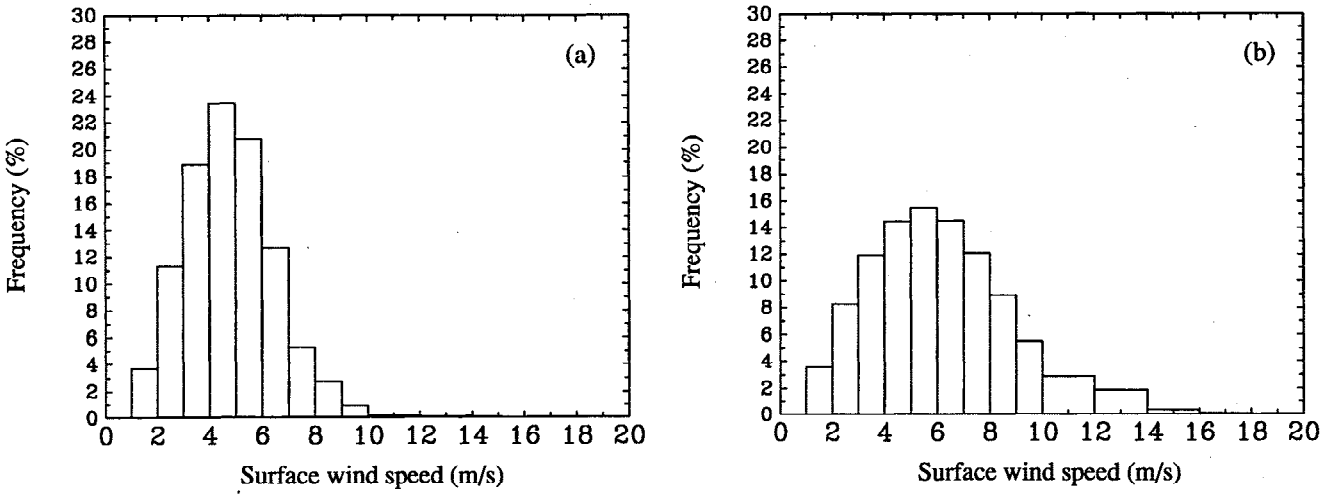

Figure 2. Surface wind speed frequency for the Saharan region for the (a) GISS GCM and (b) ECMWF 10 m wind speed products.

cycle of both the mean GCM (Figure 2a) and 1990 ECMWF (Figure 2b) surface wind speeds. Although the annual mean wind speed is approximately the same for both distributions, more high wind events occur in the ECMWF product. Because the dust emissions increase non-linearly with surface wind-speed, peak wind speed events are responsible for a major part of dust deflation. The less frequent high-wind events in the GCM compared to the ECMWF values leads to an underestimate of dust emission. To reduce this difference, we chose a threshold velocity for each land grid box in the GCM that results in the same dust fluxes compared to the off-line model with ECMWF surface winds (for which the threshold velocity was equaled 6.5 m s^{-1} at all locations). The resulting threshold velocities for surface wind speed vary between 4 and 10 m s^{-1}. It should be mentioned that due to the coarse temporal resolution of the ECMWF surface wind product with 6-hour resolution, we probably still underestimate the number and velocity of peak surface wind speed events. This leads to an underestimation of Saharan dust emission during northern hemisphere summer.

As described by *Tegen and Fung* [1994], dust is removed from the atmosphere by gravitational settling, turbulent mixing in the first model layer, and subcloud wash-out which was calculated using GCM precipitation. The difference in dust concentrations calculated with climatological precipitation compared to GCM precipitation is negligible. The efficiency of aerosol removal by rain is often described by the scavenging ratio Z, which is defined by

$$Z = C_{\text{rain}}/C_{\text{air}} \tag{2}$$

where C_{rain} is the concentration in rain in grams of dust per kilogram of rainwater and C_{air} is the aerosol concentration in air in units of grams of dust per kilogram of air. Here the wash-out of dust is calculated using a scavenging ratio of 700 as in the work of *Tegen and Fung* [1994].

We first integrated the GISS GCM for 16 model years in which the dust sources were calculated using GCM prognostic variables (experiment A). In a second experiment, designed to eliminate the effect of dust source variations upon atmospheric dust concentration, we integrated the GCM for 16 model years with fixed dust sources; that is, monthly dust fluxes were identical for each model year (experiment B). Each GCM experiment had a spin-up period of 1 model year that was discarded, so that our analysis is based upon the final 15 years.

3. Results and Discussion

3.1. Seasonal Distribution and Variability

Figure 3 shows the seasonal dust distribution averaged over the final 15 years, from experiment A with model-predicted variable dust sources. Observed features like the seasonal shift of the Saharan/Sahelian dust plume, the summer maximum over the Arabian Sea, and the spring maxima of Chinese and North American dust are well reproduced. The total GCM dust emission (of particles less than 8 μm) is 940±20 Mt/yr (mean plus or minus one standard deviation, based on monthly means) which lies within the range of current estimates [*Duce*, 1995]. The model appears to overestimate dust production in Australia which may be related to overestimating the contribution of undisturbed sources to the dust load. Another problem is that the dust source in the Sahelian/Saharan region during NH summer seems too weak compared to observations [*Prospero and Nees*, 1986; *Schütz et al.*, 1981]. This problem also occurs in the off-line version of the dust transport model as well as in other dust transport models [e.g., *Dentener et al.*, 1996; *Joussaume*, 1990]. In the GISS GCM this discrepancy could be caused by the trade winds being too weak compared to observations [*Miller and Jiang*, 1996], which may reflect problems in the parameterization of the planetary boundary layer.

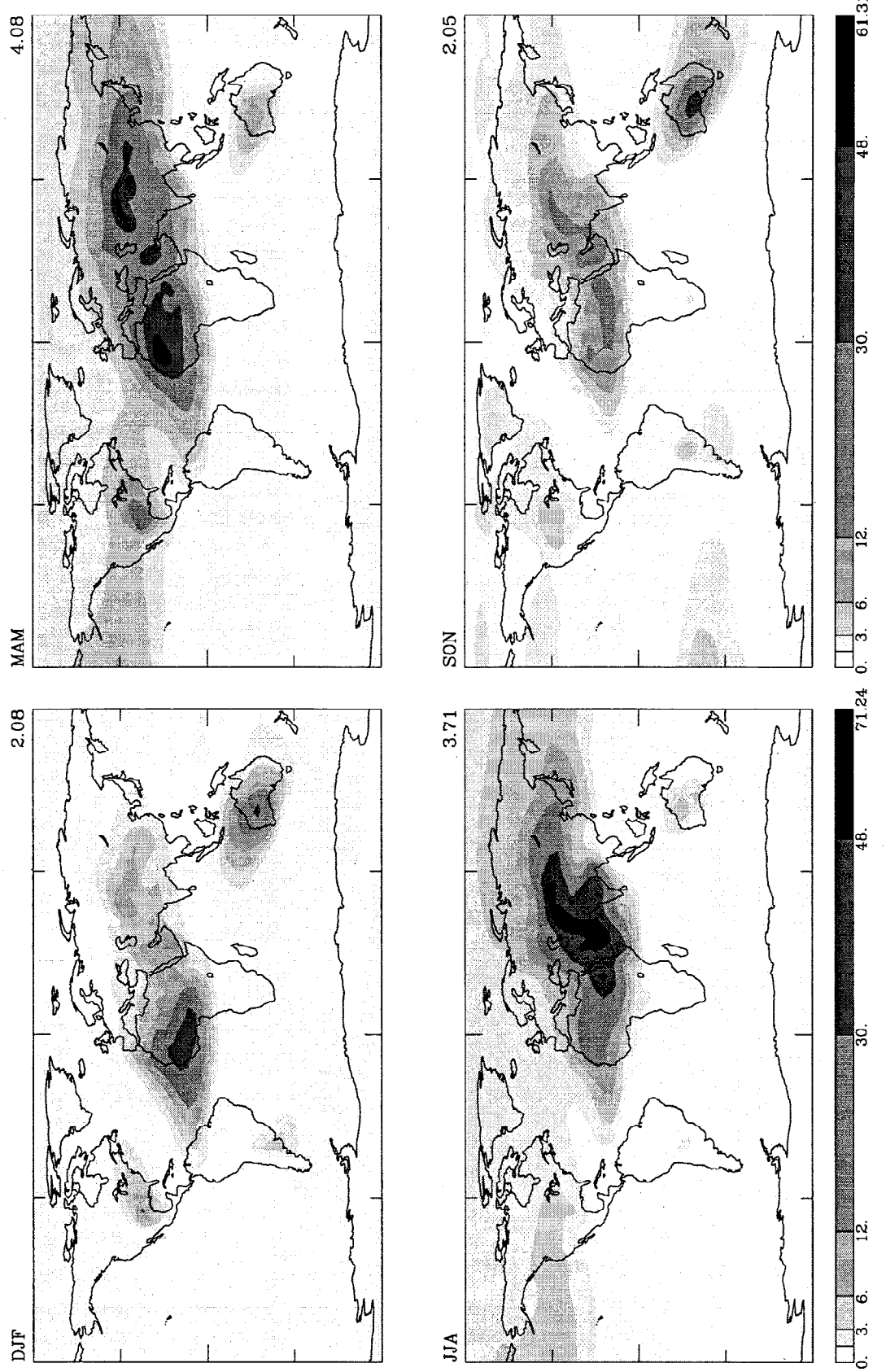

Figure 3. Dust distribution (mean concentration) calculated by the GISS GCM for the four seasons.

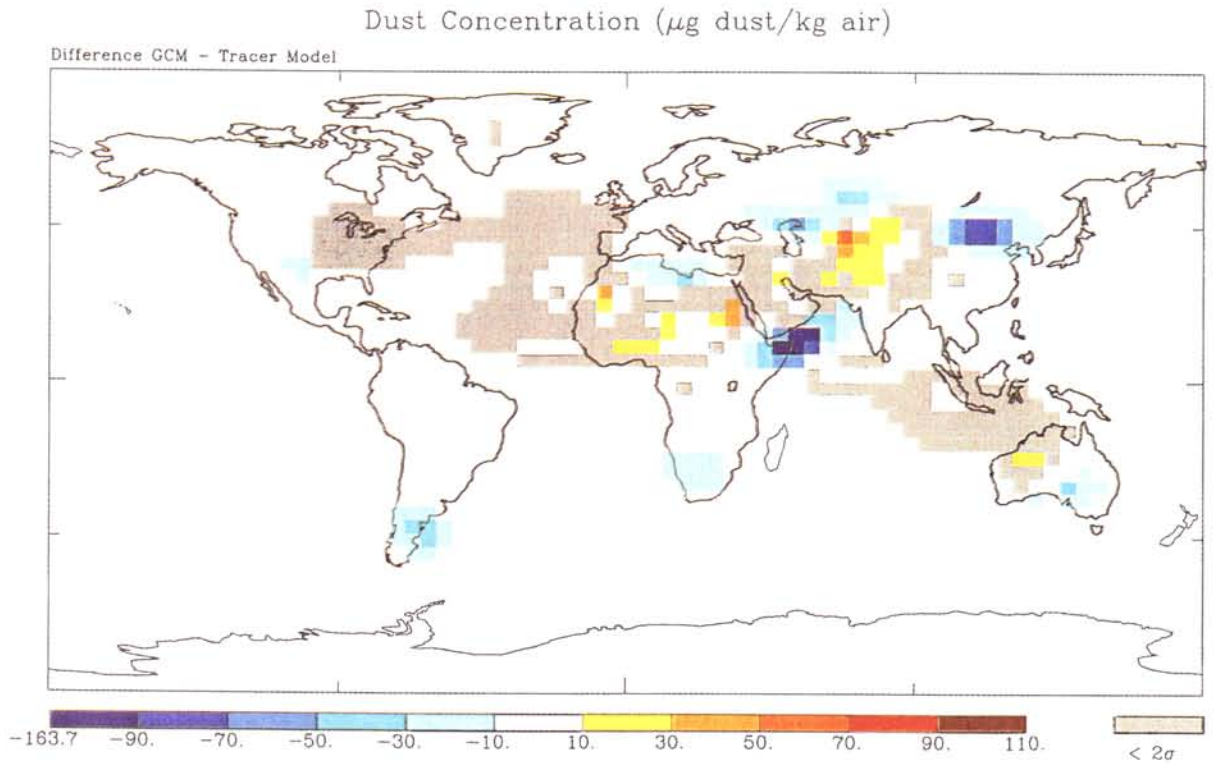

Plate 1. Difference of the annual mean dust concentration resulting from the GISS GCM and the off-line tracer model. Areas where the difference is smaller than 2 standard deviations are marked in grey.

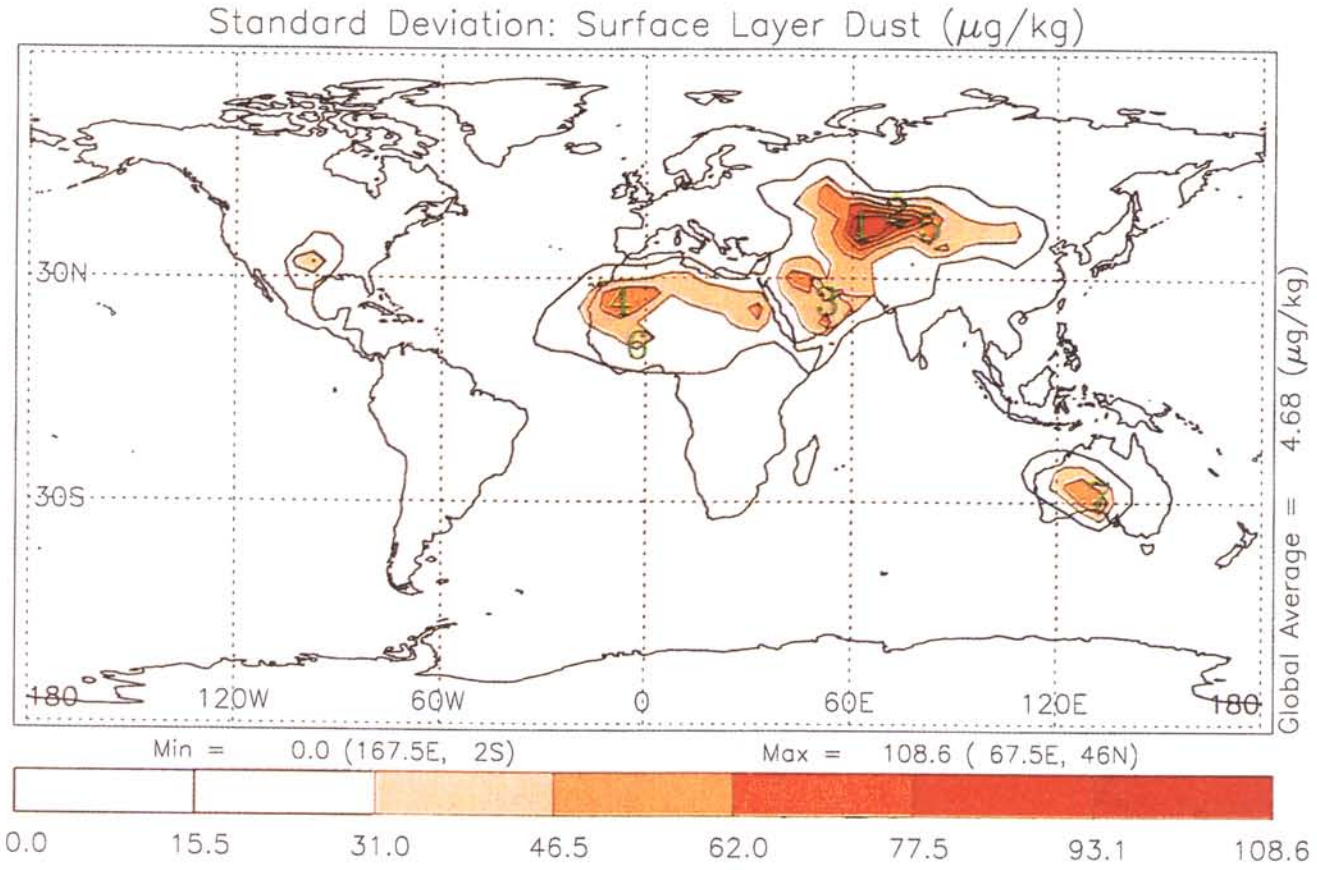

Plate 2. Annual average of the standard deviation of dust concentration within the lowest model layer. Monthly anomalies are defined with respect to the mean seasonal cycle. The numbers correspond to the region of maximum amplitude of the first seven EOFs of lowest layer dust.

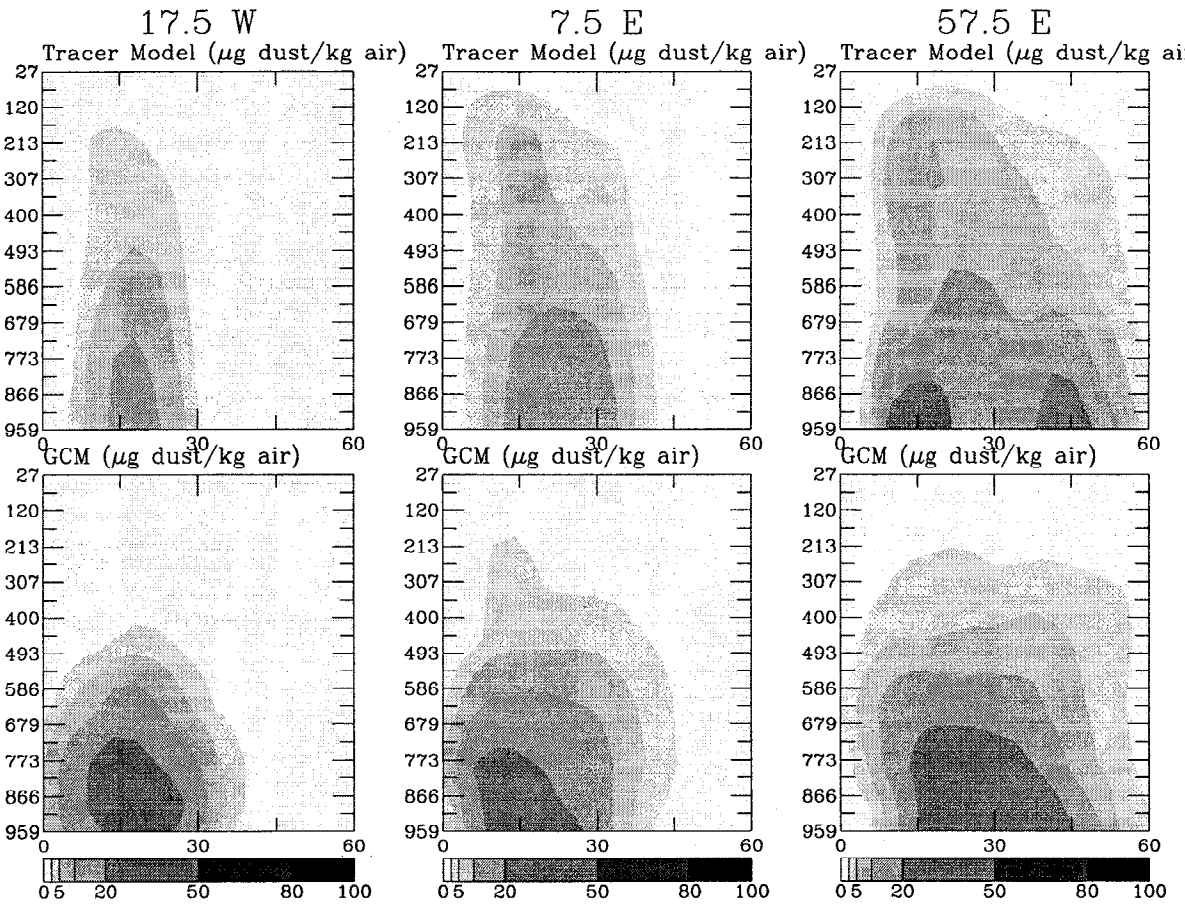

Figure 4. Comparison of the vertical distribution of clay (dust particles < 1μm) for three latitudinal cross sections (at 17.5°W, 7.5°E and 57.5 °E) from GCM and off-line tracer results.

Since no global dust climatology from observations exists (which is partly due to the high spatial and temporal dust variability and short atmospheric lifetimes of dust particles), we compare the GCM results with previously published dust distributions from the off-line tracer model [*Tegen and Fung,* 1995]. (Later, we will compare the results to satellite retrievals and ground observations.) The off-line results have been compared to observations and have been used as dust climatology in various publications [e.g., *Tegen et al.,* 1996, 1997] Plate 1 shows the difference of the annual mean first layer dust concentrations between the 15-year average of the GCM and the off-line tracer model. Areas where the differences in the dust concentration are smaller than 2 standard deviations of the GCM results are marked in grey. Over the Sahelian/Saharan source region and the Aral Sea region the GCM gives higher dust concentrations compared to the off-line tracer model (in some regions an increase of more than 100%), while significantly less dust is emitted from Somalia, South America, and China. The concentration over remote areas is smaller due to the higher wash-out efficiency. There dust concentrations can be up to 70% smaller than the off-line model results. However, since those values are small (usually less than 1μg dust per kg air), this difference is of no consequence for studies of dust climate effect. The Saharan/Sahelian dust plume extends farther south into the tropical Atlantic in the GCM compared to the off-line model results, which is due to the improved wind fields in the current GISS GCM. Although there are some significant differences between the results of the GCM and the off-line tracer model, the performance of the dust tracer in the GCM is satisfying, especially considering that no observations exist to verify dust distributions for large areas of the world.

The latitudinal and vertical cross section of the dust distribution for particles less than 1μm radius (clay) is shown in Figure 4 at three locations (17.5°W, 7.5°E, 57.5°E) in GCM and off-line tracer model. As stated by, for example, *Miller and Tegen* [1998], the radiative effect of dust is sensitive to its vertical distribution. Although measurements of vertical dust distribution in tropical regions are scarce, it is suspected that the off-line model overestimates the clay concentration in the upper atmospheric layers in these regions, since wash-out by convective precipitation is not synchronous with vertical transport by convective mixing. In reality, it can be expected that during convective mixing, dust particles are partly removed by convective rainfall. The figures show that the clay particles in the GCM are not transported as high in the troposphere as in the off-line result because precipitation and convective mixing occur at the same time step.

The unforced variability of the dust distribution in

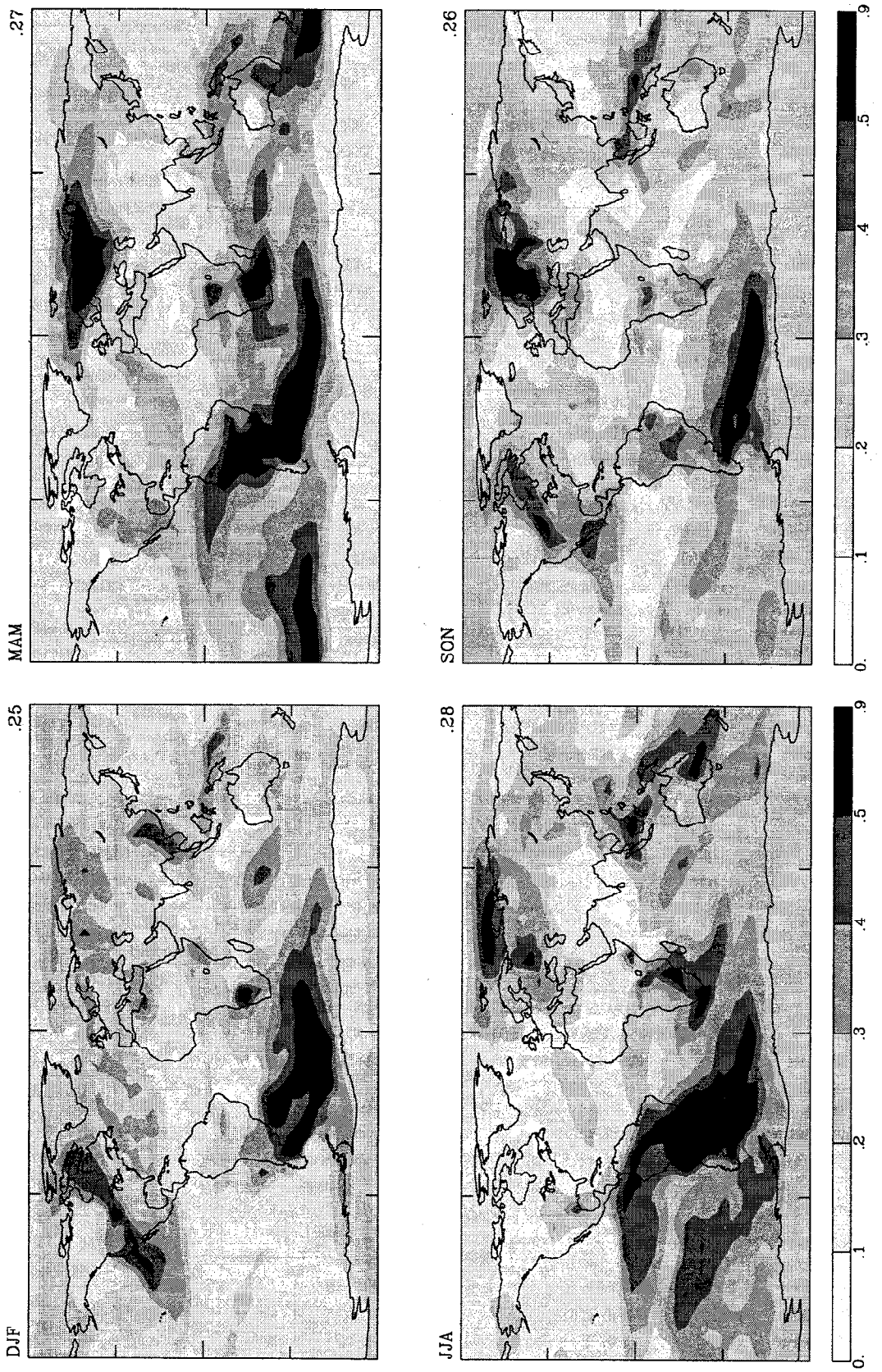

Figure 5. Ratio of standard deviations of the modeled dust for experiment A and the mean dust concentration at each model grid box.

the GCM is high, reflecting the unforced variability or "chaotic" behavior of the GISS GCM prognostic variables. We calculated for each month and each model grid box the standard deviation of the monthly mean first layer dust concentration for the final 15 years of the experiment. We then calculated the ratio of this monthly standard deviation to the monthly mean first layer dust concentration to obtain a measure of the interannual dust variability in the model. Figure 5 shows the seasonal average of this ratio for experiment A. This ratio is a measure of the intrinsic or natural variability of dust in the GCM with a given SST as lower boundary condition. Very high variability can occur in areas where the mean dust concentration is very low, like the Southern Oceans. The variability of dust concentration over the North Atlantic calculated with climatological SSTs in the GCM is comparably high. The annual average standard deviation (based on monthly means) of first layer dust concentration at Barbados (which is the location of a long-term dust record [*Prospero and Nees*, 1986]) is 25% of the mean concentration at this location for the 15-year GCM run. For individual months the dust concentration in the first model layer can vary by an order of magnitude for different GCM years. The main contribution of dust arriving at this location consists of dust from Saharan/Sahelian sources. However, the high model variability in upwind dust concentrations over the North Atlantic limits the possibility of using the GCM with given SST to predict dust concentrations in this region for individual years and thus derive information from measured dust concentrations at this location regarding possible changes in North African dust sources (due to human impact or climate change). It is tempting to attribute such observed changes in dust concentration to changes in to specific changes in precipitation or wind patterns. However, since the model shows that the "natural" variability of dust aerosol is high in areas like the North Atlantic where such changes are observed, the signal-to-noise ratio may be too high to draw such conclusions from limited time series.

3.2. Attribution of Dust Variability to Transport and Source Variabilities

An important question is whether the dust load in the atmosphere has changed due to human impact during the last decades. To investigate whether such trends exist, changes in dust source strength need to be detected which requires an estimate of source variability for comparison. To distinguish between variability in dust sources versus variability in transporting wind systems (and deposition by precipitation), we show in Figure 6 and in Table 1 the contribution of transport and deposition to the variability for experiments A (variable sources) and B (fixed sources) for the global mean and for several specific locations. Those locations are of interest because either long-term dust records exist (Barbados, Hawaii, Midway, Izania), ice core records exist which contain evidence of past dust distributions (Greenland, Antarctica), or high seasonal dust concentrations are found (North Atlantic, Mediterranean, China, North Pacific). Table 1 shows 15-year annual mean dust concentrations (a weighted average over all model layers) and standard deviations σ for experiments A and B, together with the ratio $s_{AB} = 100\frac{\sigma B}{\sigma A}\frac{\text{mean}A}{\text{mean}B}$ which we use as an estimate of the rela-

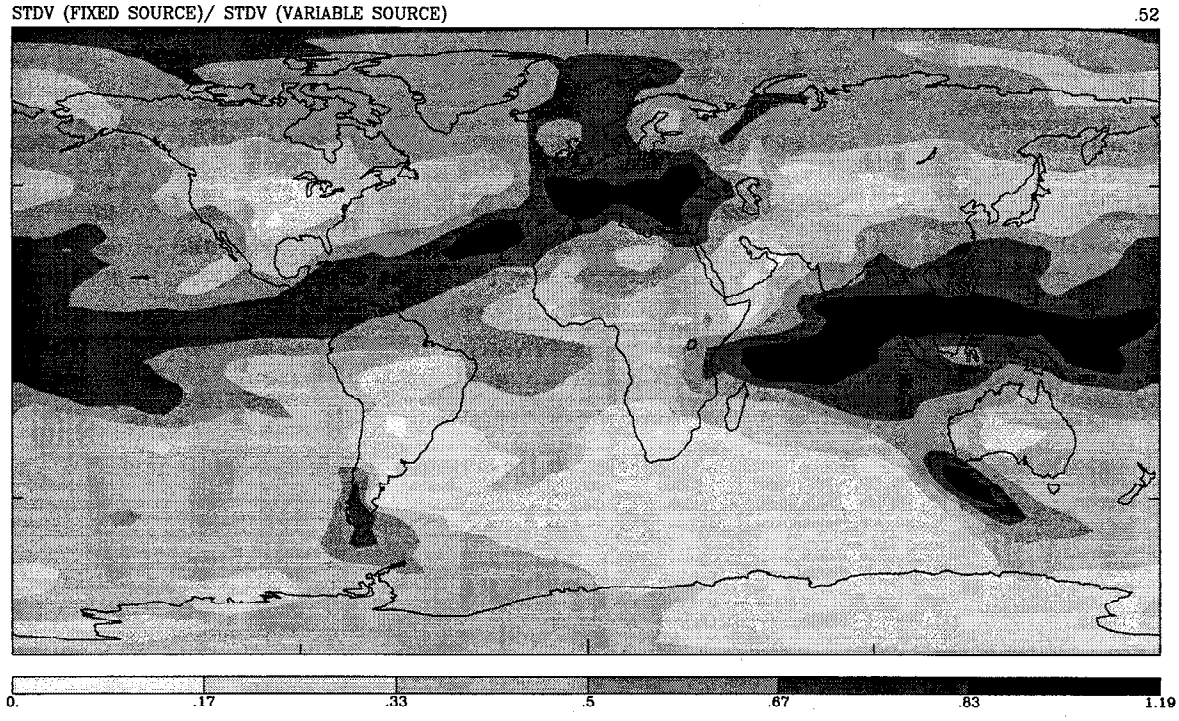

Figure 6. Percent of dust variability attributable to variability in dust transport calculated as $100\frac{\sigma A}{\sigma B}\frac{\text{mean}B}{\text{mean}A}$.

Table 1. Model Results (15 Year Runs) for Specific Locations for Mean Dust Concentrations, Standard Deviations σ of the Monthly Mean Dust Concentrations, and the Percentage of Dust Variability Attributable to Dust Transport (s_{AB})

Location	Mean A[a], μg dust/kg air	σ A μg dust/kg air	Mean B[b], μg dust/kg air	σ B, μg dust/kg air	s_{AB}[c] DJF, %	s_{AB} MAM, %	s_{AB} JJA, %	s_{AB} SON, %	s_{AB} ANN, %
Barbados	2.3	0.48	1.8	0.2	83	78	95	49	78
Izania	13.6	2.2	11.0	1.3	73	77	69	61	74
Turkey	6.8	1.2	5.6	0.9	112	84	89	73	87
China	6.6	0.9	5.7	0.4	36	51	72	76	56
Cheju	5.8	0.8	5.0	0.4	50	36	63	91	53
Oahu	0.9	0.1	0.9	0.1	46	75	67	67	68
Greenland	1.6	0.2	1.4	0.1	37	56	83	35	58
Antarctica	0.2	0.0	0.1	0.0	19	35	78	25	31
NE Atlantic (30W-0E;0N-20N)	14.6	1.8	11.4	0.6	43	48	53	49	44
NE Atlantic (30W-0E;20N-40N)	11.6	1.7	10.6	0.9	76	75	75	63	73
Mediterranean	5.9	1.1	6.1	0.8	105	85	78	65	82
Arabian Sea	16.3	1.8	20.2	0.8	54	62	42	44	45
NW Pacific (120-150E;30-50N)	5.5	0.8	5.4	0.3	45	43	45	61	46
SW Pacific (100-170E;25-45S)	2.9	0.6	1.5	0.1	64	56	57	44	50

[a]Experiment A: variable dust sources.
[b]Experiment B: fixed dust sources.
[c]$s_{AB} = 100 \frac{\sigma B}{\sigma A} \frac{\text{mean A}}{\text{mean B}}$.

tive contribution of dust transport to the dust variability at the each location. This ratio is is based on a relatively small statistical sample; therefore values larger than 100 can occur (although such values would not be physically meaningful). s_{AB} is given for the four seasons together with the annual mean weighted with monthly dust concentrations, calculated as $s_{AB}(ANN) = \sum_{i=1}^{12}(s_{ABi}c_i)/\sum_{i=1}^{12} c_i$ where c_i is the monthly mean dust concentration at each location. (The contribution of the source variability would be $(100-s_{AB})$ in each case.) Figure 6 shows the variability attributable to transport as an annual mean, weighted with the monthly mean dust concentration at each model grid box (i.e., months with higher dust concentrations contribute more to the average). The part of dust variability that is attributable to transport variability rather than source variability varies widely for the different locations and for different seasons. Generally, the contribution of source variability tends to be stronger closer to source areas than in remote areas (as expected), while in the southern hemisphere the source variability has a stronger contribution to the modeled dust variability than in the northern hemisphere.

At the locations Barbados and Izania in the North Atlantic, 70-80% of the dust variability in the model is attributable to transport variability, the values being higher at Barbados which is located farther away from the Saharan/Sahelian dust sources. Similar values of $s_{AB} \approx 75\%$ can be found over the North Atlantic between 20°N and 40°N for all seasons except northern hemisphere fall. Farther south at 0°N–20°N, s_{AB} has lower values of about 43% in winter and 50% in the other seasons, which means that the variability in sources contributes more to the dust variability at these latitudes. It should be noted that since for these calculations the GCM was integrated with fixed SSTs, additional variability in dust concentration can be expected from variations in external forcing such as SST related to the North Atlantic Oscillation (NAO), for example. Over the Mediterranean and Turkey (where dust has been transported across the Mediterranean from the Saharan desert), the variability in dust transport is high especially in the winter months, where all variability in dust concentration can be attributed to variations in transport. The weighted annual mean s_{AB} at these locations lies between 82 and 87%, meaning that the dust load at these locations is mainly controlled by transport in the model. Over the Arabian Sea (where the highest dust loads are found in the northern hemisphere summer), variability of sources and transport contribute in approximately equal parts to the interannual dust variability, reflecting the relatively high contribution of source variability in the summer months. Over the North Pacific and at the locations China and Cheju, dust variability can again be attributed in equal parts to source and transport variability. Cheju shows a contribution from transport variability of only 36% in the northern hemisphere spring when the maximum dust loads are observed. In the Pacific between 30°N and 50°N, dust source variability contributes strongly to dust variability. Farther south, the transport variability is the main contributor. Over the southwest Pacific in the vicinity of Australia, about 50% of the interannual dust variability can be explained by transport variability in the model.

At the remote regions Greenland and Antarctica, where ice core records provide information about long-term changes in dust deposition, s_{AB} varies strongly with the season. In Antarctica, where maximum dust concentrations in the model occur in the southern hemisphere spring and summer, the source contribution to the interannual dust variability is relatively strong. Here only about 20-30% of the variability is attributable to transport variability in the months with high dust loads. In Greenland, sources and transport contribute equally to the interannual dust variability, with transport dominating in the months with the strongest dust loads (late spring/early summer). These values give an indication at which locations changes in dust sources (caused by either human impact or changes in climatic conditions) might be detected most easily by long-term observations. At locations like the Mediterranean, where the interannual dust variability is dominated by transport variability, detection of changes in the dust source strength would be very difficult. It would be easiest to detect changes in the Saharan/Sahelian dust sources from measurements at lower latitudes in the North Atlantic, where the transport contribution to the interannual dust variability is small. Cheju appears to be a good location to observe changes in Asian dust sources.

3.3. Comparison With AVHRR Aerosol Optical Thickness Retrievals

Dust aerosol optical thickness was calculated from the modeled dust mass and size distributions as described by *Tegen and Fung* [1994]. Figure 7 shows the results of the GCM dust optical thickness for 10 model years (the limitation to 10 years was chosen to avoid overcrowding of the figure) of experiment A compared to optical thickness retrievals from the NOAA advanced very high resolution radiometer (AVHRR) satellite [*Rao et al.*, 1988] at six ocean locations where a high contribution of dust to the aerosol optical thickness is expected. The model provides an extinction optical thickness, which is equivalent to the scattering optical thickness if the aerosol is assumed to be nonabsorbing. In fact, dust particles partly absorb solar radiation; therefore satellite values should be regarded as lower limits for the extinction optical thicknesses in regions of high dust concentration, since in this version of AVHRR retrievals it is assumed that dust is totally reflecting (single scattering albedo of 1). Another source of uncertainty is the different size distribution assumed by the AVHRR satellite retrievals [*Stowe et al.*, 1997] and the model; in the latter the size distribution is computed dynamically and is different for each grid box. In regions where other aerosol types besides dust are present, the modeled optical thicknesses are expected to be lower than the satellite retrievals. Although together these uncertainties

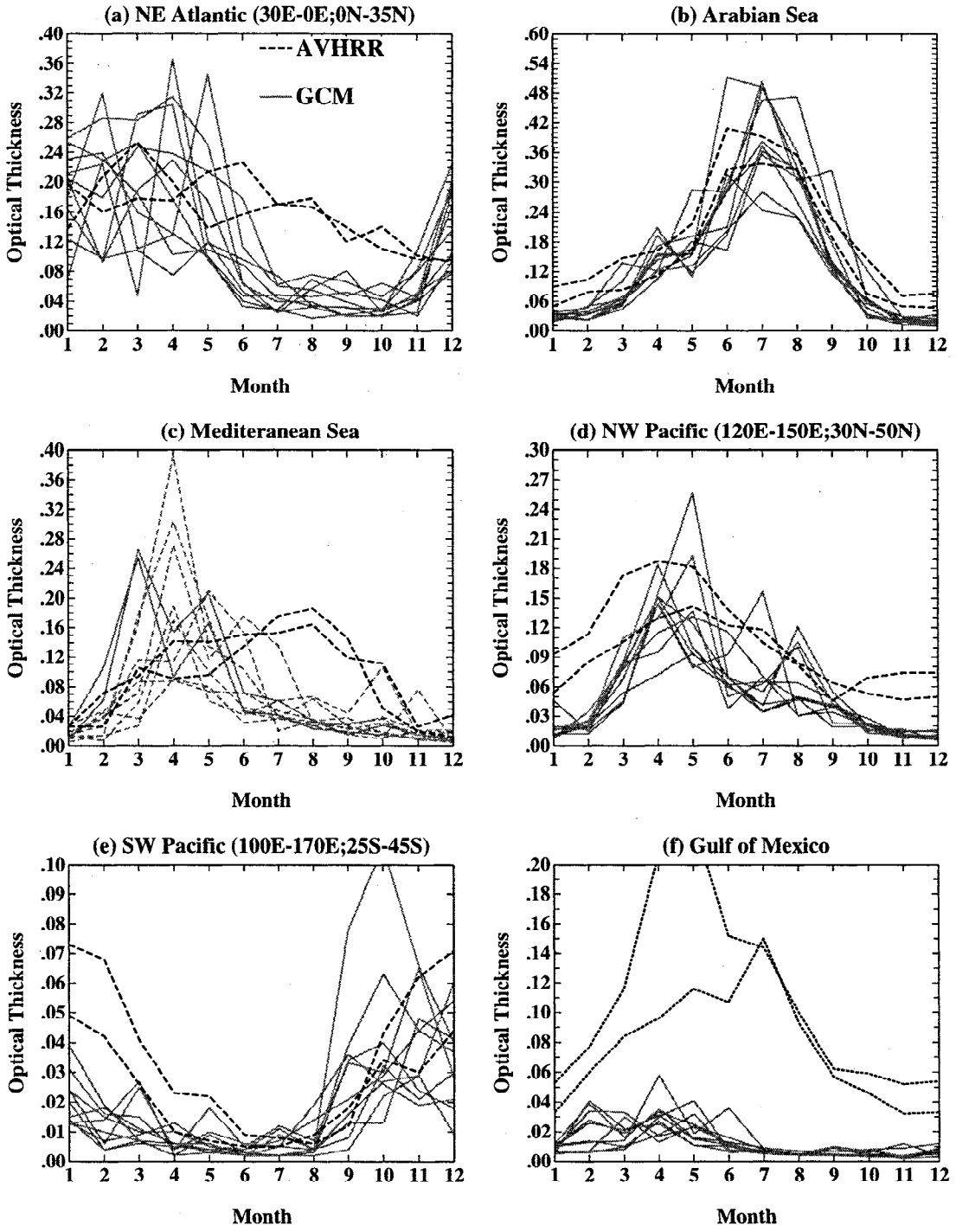

Figure 7. Comparison of dust optical thickness of 10 model years with AVHRR retrievals of optical thickness in regions with strong dust contribution to the aerosol load.

make a direct comparison between model results and retrieved optical thicknesses problematic, such a comparison still can be useful to indicate regions where the model-derived optical thicknesses are inconsistent with the observations.

The magnitude and seasonal cycle of dust is well reproduced in the Arabian Sea (Figure 7b) and the Pacific (Figures 7d and 7e) locations. Over the North Atlantic (Figure 7a) the model underestimates dust in the Northern Hemisphere summer months. In the Mediterranean (Figure 7c) the modeled dust maximum is in April instead of the northern hemisphere summer (when AVHRR retrievals find an optical thickness maximum), which may be due to a higher contribution of industrial aerosols in the summer months. In the Gulf of Mexico (Figure 7f) the dust optical thickness from the model is much smaller than the AVHRR values; here we apparently have a strong contribution of industrial aerosols to

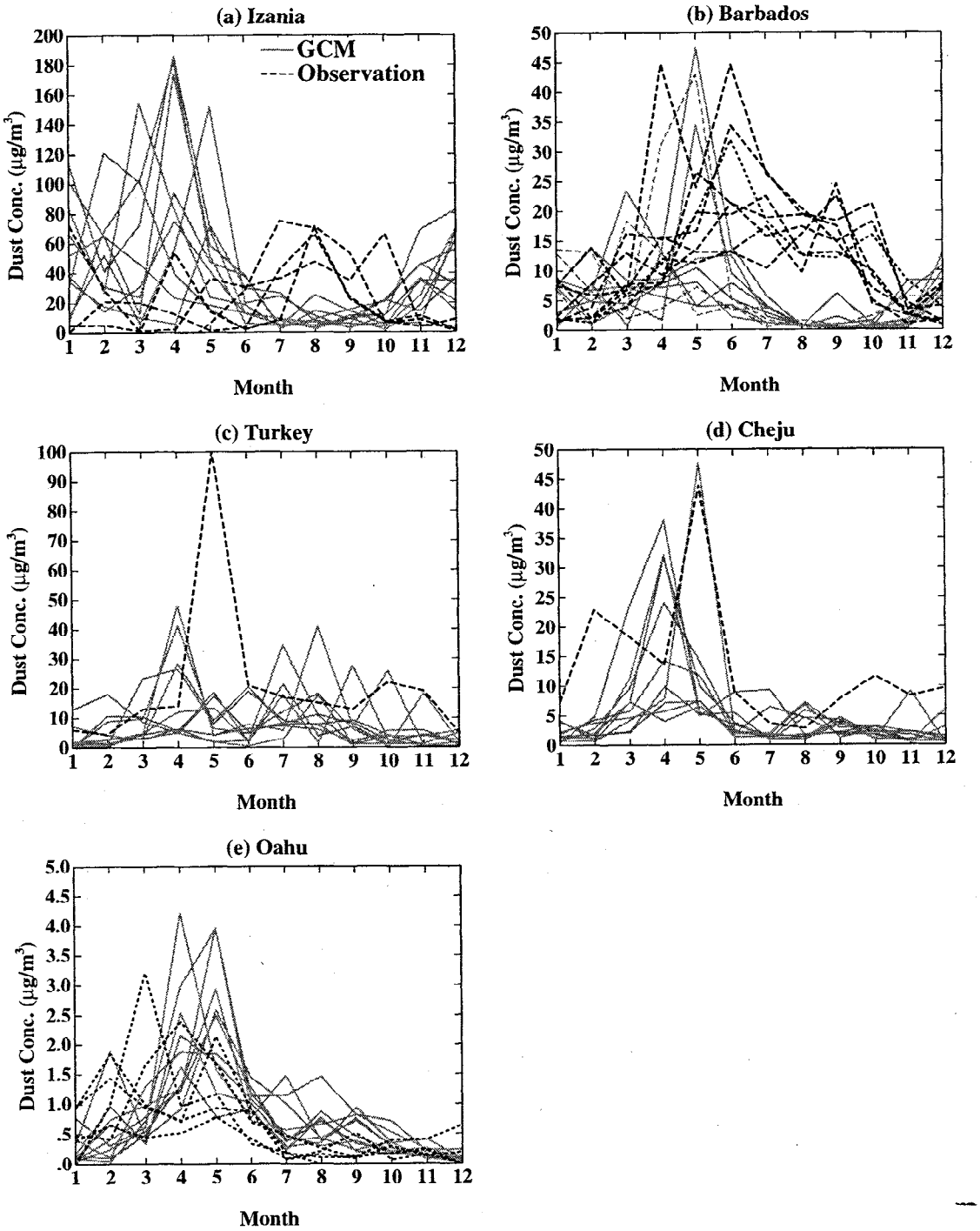

Figure 8. Comparison of first atmospheric layer soil dust concentration from 10 GCM years with surface observations.

the optical thickness. Also for the NW Pacific (Figures 7c and 7d) locations, the presence of industrial (and biomass burning) aerosols could cause an underestimation of modeled compared to retrieved optical thickness.

The interannual variability of the modeled dust varies with location. While over the Arabian Sea the dust optical thickness is relatively constant each year, over the Mediterranean and the North Atlantic (during winter and spring), the year-to-year variations of the dust load can be extremely large. Even the month of maximum dust optical thickness can change from one year to another. Therefore, when comparing model results with only 1 or 2 years of observations, discrepancies can always be expected.

3.4. Comparison With First Layer Dust

Figures 8a-8e show a comparison of the dust model results for the first (i.e., lowest) model layer with ground-based measurements at different locations (measurements from J. Prospero and D. Savoie, Rosenstiel School

Table 2. Summary of the First Seven EOFs of Surface Layer Dust Concentration (Which Together Represent 54.1% of the Total Variance), the Season of Peak Amplitude, and Their Correlation With Anomalies of Surface Wind Speed and Precipitation.

EOF	Location	Variance, %	Season	$\|u_s\|$ Correlation	Precipitation Correlation
1	Eurasia	14.7	June–Aug.	0.26	-
2	Eurasia	7.9	April–July	-	-0.21
3	Arabia	7.7	June–Aug.	0.39	-0.17
4	Western Sahara	7.3	April–June	0.53	-0.41
5	Mongolia	6.9	April–Aug.	0.36	+0.21
6	Sahel	4.8	Dec.–March	0.54	-0.47
7	Australia	4.8	Sep.–Feb.	-	-0.37

For the time series associated with each EOF, the lag autocorrelation falls to near zero within 1 or 2 months. If each month is assumed to be independent, the correlation of the EOF time series with a random series will exceed 0.15 only 5% of the time. Small correlations have been omitted from the table using this criterion.

of Marine and Atmospheric Sciences, Miami, Florida; measurements from Turkey from N. Kubilay, Nilgun Kubilay, Middle East Technical University, Turkey). The interannual variability of the first layer concentrations is generally higher than the optical thickness variability. As with dust optical thickness, the model underestimates dust concentrations in the northern hemisphere summer at the North Atlantic stations Izania (Figure 8a) and Barbados (Figure 8b). During spring the model seems generally to overestimate dust concentration at Izania while the winter and spring model results at Barbados reflect the range of the observed concentrations, including the large variability. At Turkey (Figure 8c) where 1 year of surface observations (1992) was available, the model dust concentrations have two peaks in spring and fall [*Kubilay and Saydam,* 1995]. The very strong peak in the dust observations in May was not reproduced. The year 1992 was a year with strong dust transport across the Mediterranean [*Moulin et al.,* 1997b] and the ground observations for the month of May may be biased because of technical problems during that month (N. Kubilay, personal communication, 1997). This may explain the discrepancy to the model results. At the Pacific locations Cheju (Figure 8d) and Oahu (Figure 8e) the model results lie in the range of the observed concentrations. Although for most model years the dust concentration at Cheju is highest in April, in 1 model year the maximum dust concentration is in May, which agrees very well with the May maximum during the single year of observations.

Again, it is noted that year-to-year variability is large in some locations with changes of an order of magnitude possible from one year to another. This again indicates the importance of multiyear observations of dust to obtain the climatological mean dust concentration.

Interannual Variability and EOFs

The standard deviation of dust concentration within the lowest model layer, shown in Plate 2, provides a typical magnitude of departures from the seasonal cycle. Variability is largest in arid regions where the mean value is also high, exhibiting a maximum in central Eurasia. While long-term dust measurements exist for many parts of the world, less attention has been given to this region, in part because many satellite retrieval methods are limited to oceanic regions. The large model variability in Eurasia suggests the value of observations in this region, for example, through Sun photometers or total ozone mapping spectrometer (TOMS) retrievals which can measure column dust amount over both land and ocean [*Herman et al.,* 1997]. The standard deviation of column-averaged dust (not shown) displays a similar geographic distribution, although with less regional concentration, as the winds which lift dust above the surface layer also cause lateral dispersion.

The standard deviation shown in Plate 2 is calculated by averaging the standard deviation of monthly anomalies relative to the seasonal cycle over all 12 months. In fact, large variability in each region is typically confined to a particular season. To identify regional and temporal patterns of interannual dust variability, we constructed empirical orthogonal functions (EOFs [see, e.g., *Kutzbach,* 1967; *North et al.,* 1982] of the surface layer dust. (The EOFs were further rotated using the varimax criterion [e.g., *Horel,* 1981], in order to reduce correlations between different regions that arise spuriously as a result of the finite length of the simulation.) The locations of the maximum amplitude corresponding to the first seven EOFs are identified by number in Plate 2. The variance associated with each mode, along with the predominant season of variability, is listed in Table 2.

The gravest two modes (i.e., the two modes representing the greatest fraction of global variance, almost one quarter according to Table 2) are located in central Eurasia. The first mode peaks during NH summer, while the second represents springtime variability. As a first step toward understanding the origin of this variability, we correlated the time series associated with each mode with the anomalous surface wind speed and precipitation. The former provides a rough measure of the frequency of high surface winds that exceed the

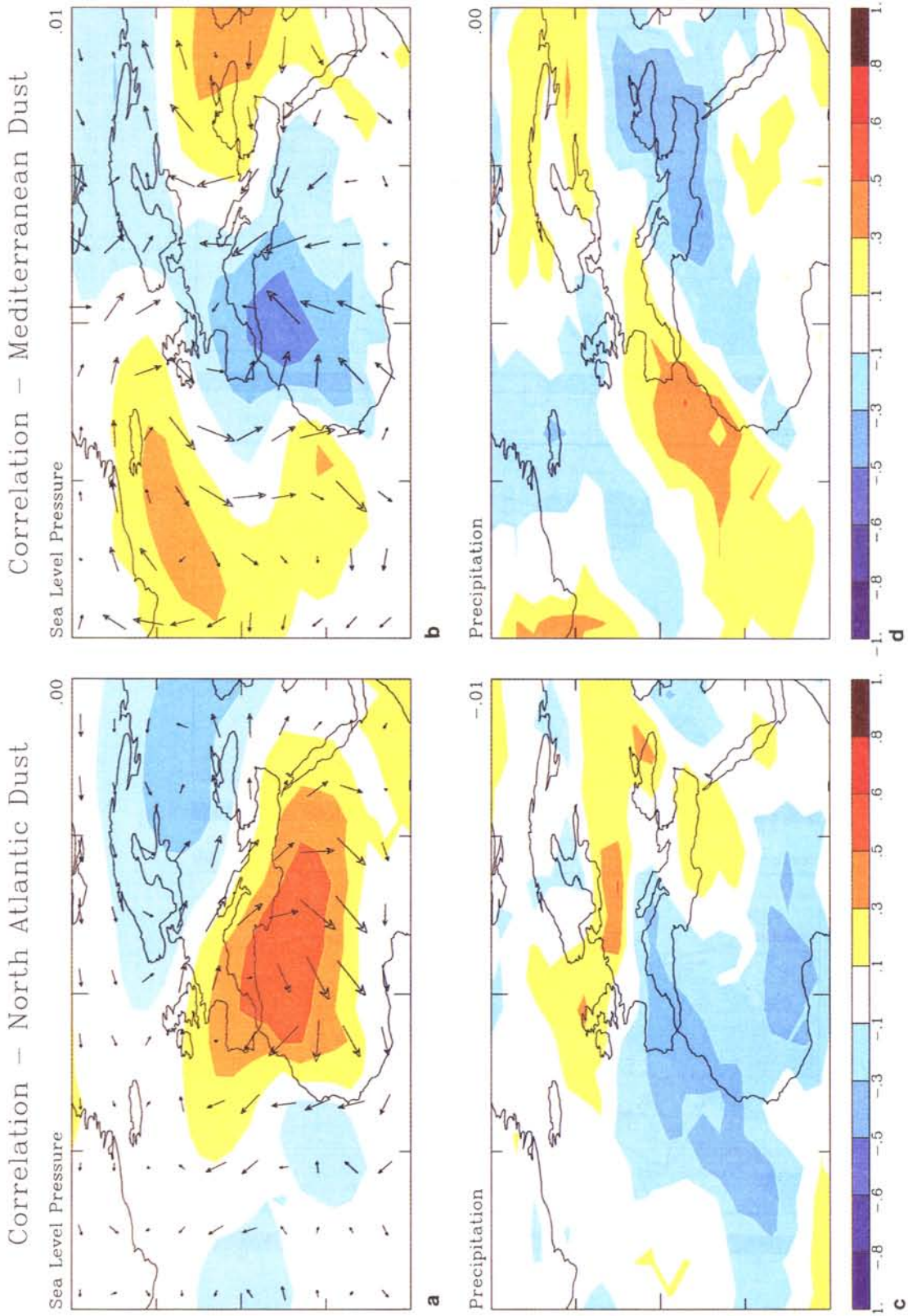

Plate 3. Maps of Correlation coefficients between dust load at specific locations and climate parameters: (a) North Atlantic dust and precipitation, (b) North Atlantic dust and sea level pressure and surface wind speed, (c) Mediterranean dust and precipitation, and (d) Mediterranean dust and precipitation.

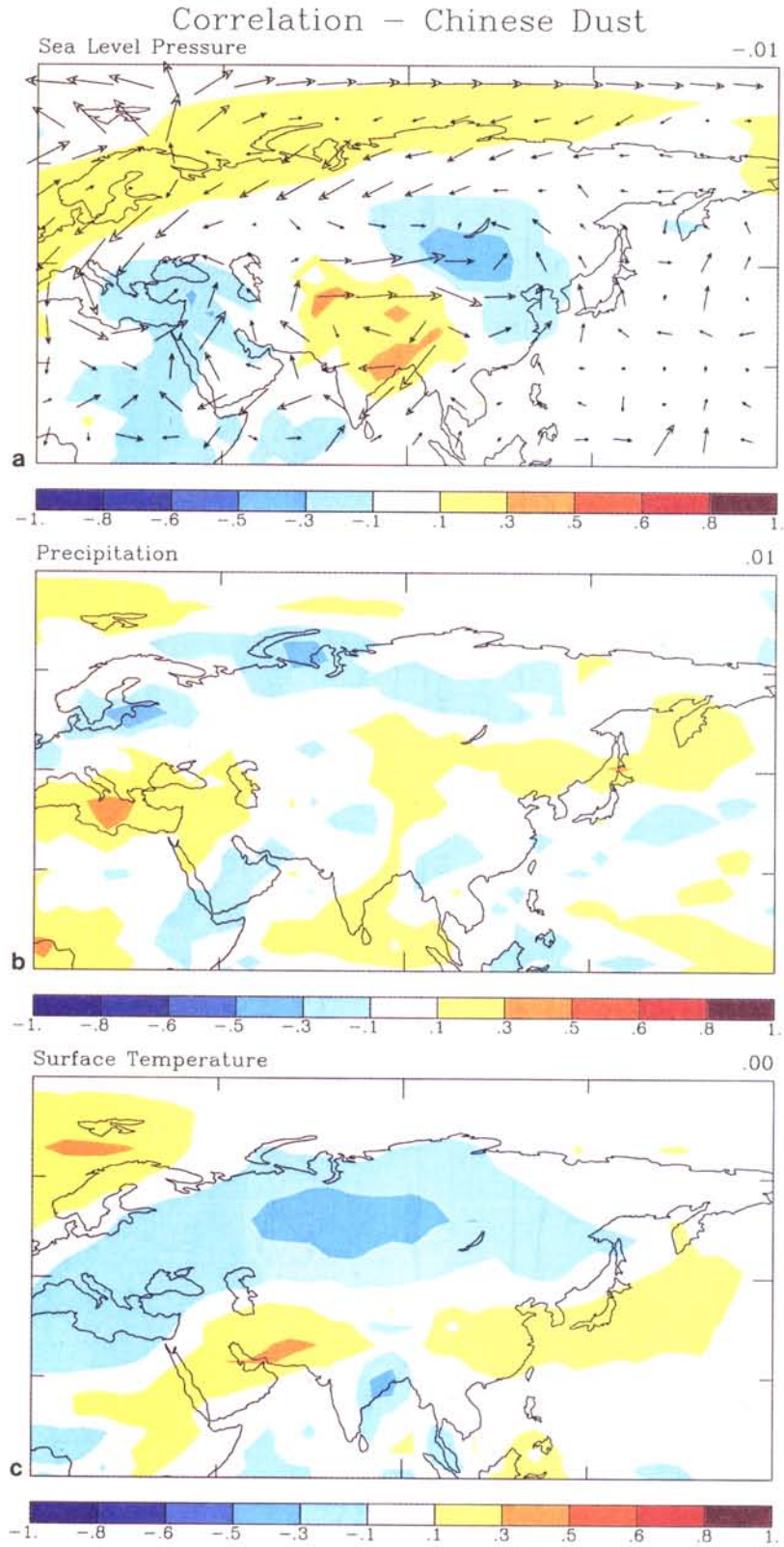

Plate 4. Correlation coefficients between dust load at Beijing and climate parameters: (a) sea level pressure and surface wind speed, (b) precipitation, and (c) surface temperature.

threshold for lofting dust into the atmosphere. A deficit of the latter can dry out the soil, expanding the source region, while reducing wet deposition of dust already in the atmosphere. Table 2 shows the largest correlation of the mode time series with respect to surface wind speed and precipitation, within two grid boxes of the EOF maximum. The summertime Eurasian mode is correlated with increased wind speed, while the spring mode is correlated with reduced precipitation. (However, the summer mode is largest 1 month after anomalous rainfall in the Indian monsoon region, displaying a correlation of 0.61.)

In several regions, including Arabia, the western Sahara, and the Sahel, increased dust emissions are accompanied by both an increase in surface winds and a reduction in rainfall. It is not clear whether both processes lead to variability of dust emissions, or whether one process dominates. Table 2 demonstrates that the model correctly reproduces the shift in dust production between the Sahel during NH winter and the Sahara in spring and summer [e.g., *Carlson and Prospero,* 1972]. However, as mentioned before, transport into the Atlantic during the NH summer is underestimated by the model, as reflected by the springtime peak of the western Sahara mode.

3.6. Dust and the NAO

According to satellite estimates of column dust by *Moulin et al.* [1997a], interannual variations in atmospheric dust over the Mediterranean and the subtropical east Atlantic are well-correlated with each other during NH summer. Dust variations are also correlated with the North Atlantic Oscillation (NAO). Both correlations are absent in the GCM during this season, which may reflect either the weak dust transport out of Africa or the absence of strong NAO variability, which might otherwise organize dust transport. During NH winter the NAO is the dominant mode of sea level pressure (SLP) variability in the model Atlantic. The leading EOF of the GCM (not shown) closely resembles the observed mode computed by *Hurrell* [1995], exhibiting the classical "dipole" spatial pattern with an amplitude comparable to that observed. However, model variations in Atlantic SLP during NH summer are dominated by a different spatial structure in this region. The absence of a model NAO during NH summer may result from the prescription of SST, which reduces the persistence of winter and springtime anomalies associated with the NAO. It is expected that the summertime NAO will be more prominent when the atmospheric model is coupled to a mixed-layer ocean, where ocean temperatures can change in response to the NAO, leading to a greater persistence of this pattern [e.g., *Lau and Nath,* 1996]. A stronger NAO may be better correlated with dust concentration.

3.7. Interannual Dust Variability on Regional Scale

For several regions (North Atlantic, Mediterranean, China) we investigated the dependency of the modeled dust concentration on meteorological parameters like precipitation, sea level pressure, and surface winds. Small-scale wind systems, which may be important for dust generation and transport, are not necessarily well reproduced by the GCM. However, we can investigate whether variations in the large-scale circulation exert some control upon interannual dust variability.

3.7.1. North Atlantic. The dust load over the North Atlantic is of particular interest, as for this region long-term observations and a few studies relating the dust load to climate parameters and modes exist. As mentioned above, a recent study [*Moulin et al.,* 1997a] found a correlation between North Atlantic dust loads (from Meteosat observations) and the North Atlantic Oscillation (NAO). In addition, *Prospero and Nees* [1986] found a correlation between the rainfall deficit in the Sahel and the concentration of Saharan dust in Barbados in the northern hemisphere summer months. The correlation of Barbados summer dust was even stronger with the Sahelian rainfall deficit of the previous year. They concluded that as a consequence of the lack of precipitation, the vegetation cover in the dust source area decreased, which would allow for stronger dust deflation. *Prospero and Nees* [1986] also related interannual changes of the winter dust concentration to changes in atmospheric transport, as they found a strong winter dust signal during the El Nino–Southern Oscillation (ENSO) years of 1982-1983.

In Plates 3a and 3b, correlation coefficients of the North Atlantic dust concentration at (20°N-40°N; 50°W-10°W) with sea level pressure (Plate 3a) and precipitation (Plate 3b) anomalies for experiment A are shown for each model grid box. The values are averaged monthly correlation coefficients which were weighted by the mean dust concentrations. In Plate 3a, additional correlation coefficients for the u and v components of the surface wind speed are shown as wind vectors. High dust concentration over the North Atlantic is correlated with a specific pressure pattern with a high-pressure anomaly located over northwest Africa and a low-pressure anomaly over northern Europe. In Table 3, the correlation coefficients between dust concentration and the pressure difference between the locations (25°N; 5°E) and (50°N; 40°E) are shown. Results are given for the different seasons for the experiments A (variable sources) and B (fixed sources). The numbers show for both cases the highest correlation coefficients of 0.64 and 0.63 for spring and the lowest for summer with 0.36 and 0.33.

The model gives a negative correlation between North Atlantic dust concentration and precipitation anomalies over the North Atlantic and the Saharan/Sahelian source region. The correlation coefficient r between North Atlantic dust concentration and the precipitation deficit over both the North Atlantic and the dust source area is shown in Table 3. Precipitation was averaged over the areas (20°N-40°N; 50°W-10°W) (North Atlantic) and (5°N - 40°N; 0°E - 30°E) (source area), respectively. The correlation coefficient r is highest for the summer months with values between 0.55 and 0.66 for the experiments A and B. The fact that the corre-

Table 3. Correlation Coefficients r of North Atlantic Dust Concentrations Averaged Over (20°N-40°N; 50°W-10°W) with Pressure Differences Between (25°N; 5°E) and (50°N; 40°E) and With Precipitation Deficits Over Both the North Atlantic and the Dust Source Area

	r DJF	r MAM	r JJA	r SON	r ANN [a]
Sea level pressure (A)[b]	0.51	0.64	0.36	0.36	0.53
Sea level pressure (B)[c]	0.49	0.63	0.33	0.37	0.51
Precipitation (A)	-0.41	-0.44	-0.56	-0.49	-0.46
Precipitation - source area (A)	-0.25	-0.26	-0.55	-0.46	-0.31
Precipitation (B)	-0.36	-0.58	-0.66	-0.38	-0.52
Precipitation - source area (B)	-0.51	-0.56	-0.63	-0.38	-0.54

Precipitation was averaged over the areas (20°N-40°N; 50°W-10°W) (North Atlantic) and (5°N-40°N; 0°E-30°E) (source area), respectively.
[a]Annual mean is weighted with monthly mean dust concentrations.
[b]Experiment A: variable dust sources.
[c]Experiment B: fixed dust sources.

lation coefficient is only slightly higher for experiment A (variable sources) than for B (fixed sources) for the North Atlantic precipitation deficit (while r is about equal for the source areas for cases A and B) indicates that in the model, transport anomalies are fundamental, while precipitation anomalies play a minor role for dust production. On the other hand, it cannot be decided whether this negative correlation in the model is due to increased dust removal by precipitation or whether the precipitation anomaly is caused by the same pressure situation that apparently causes stronger dust transport. The model correlation is smaller than the observed correlation between the Saharan dust collected at Barbados and the Sahelian rainfall deficit, where *Prospero and Nees* [1986] found an annual correlation coefficient of 0.75 and a significantly higher correlation with respect to the rainfall deficit of the previous year.

3.7.2. Mediterranean. Mediterranean dust concentration in the model is correlated with a negative pressure anomaly over northwestern Africa (Plate 3c). For variable dust sources (A) this negative correlation between Mediterranean dust concentration and the maximum pressure difference between the locations (30°N; 5°W) and (55°N; 30°W) is strongest in the northern hemisphere spring (Table 4), while for fixed sources, r is largest in the winter. The cyclonic flow associated with low pressure over Morocco/Algeria causes northward dust transport from the Sahara in the model. Such dependency of northward transport of Saharan dust on the location of the cyclonic center has been explained by *Bergametti et al.* [1989]. The annual mean correlation coefficients are -0.54 and -0.37 for the prognostic and fixed source experiments, respectively. In the model the Mediterranean dust is also negatively correlated with precipitation anomalies over the Mediterranean (Plate 3d and Table 4), with correlation coefficients of -0.34 and -0.41 in the annual mean, although in specific seasons (summer in the case of variable sources) the correlation is weak with a coefficient of only 0.09. Again, it appears that the Mediterranean dust load is not influenced by changes in source strength, as the GCM run with fixed sources show similar results compared to the run with variable sources (where a decrease in precipitation potentially leads to an increase in dust fluxes). Negative correlation between dust concentration and the precipitation deficit could be either a consequence of the pressure patterns, or variations in the wash-out rates that are a controlling factor for the dust variability.

3.7.3 China. Long-term observations of dust storm frequency in China exist, although it is difficult to attribute the year-to-year dust variability to specific factors. *Goudie and Middelton* [1992] found only a weak correlation ($r = -0.03$) between annual rainfall and dust storm frequency, while *Littmann* [1991] found a stronger correlation with $r = -0.26$ between dust storm frequency and monthly mean rainfall. The stronger correlation for monthly precipitation can be attributed

Table 4. Correlation Coefficients r of Mediterranean Dust with Pressure Differences Between (30°N; 5°W) and (55°N; 30°W) and with Precipitation

	r (DJF)	r (MAM)	r (JJA)	r (SON)	r (ANN)
Sea level pressure (A)	-0.39	-0.68	-0.38	-0.44	-0.54
Sea level pressure (B)	-0.74	-0.33	-0.34	-0.64	-0.37
Precipitation (A)	-0.08	-0.48	-0.09	-0.32	-0.34
Precipitation (B)	-0.03	-0.58	-0.28	-0.33	-0.41

See Table 3.

Table 5. Correlation Coefficients r for the Individual Seasons Between the Dust Concentration at Beijing and the Sea Level Pressure Differences Between the Locations (50°N; 110°W) and (75°N; 60°E), the Precipitation Deficit in the Area (30°N-50°N; 90°E-110°E), and the Surface Temperature in the Area (50°N- 60°N; 50°E -100°E) for Experiments A and B

	r (DJF)	r (MAM)	r (JJA)	r (SON)	r (ANN)
Sea level pressure (A)	-0.38	-0.41	-0.37	-0.46	-0.38
Sea level pressure (B)	-0.61	0.09	0.08	0.15	0.04
Precipitation (A)	0.19	-0.01	-0.39	-0.10	-0.11
Precipitation (B)	-0.25	-0.57	-0.33	-0.50	-0.46
Surface temperature (A)	-0.36	-0.38	-0.34	-0.44	-0.37
Surface temperature (B)	-0.46	0.03	0.22	0.18	0.05

See Table 3.

to the fact that dust storms in China occur mainly in spring which is the driest season. However, precipitation deficits apparently do not play a major role in interannual changes of dust storm frequency. On the other hand, *Zhang* [1984] found a correlation of $r = -0.59$ between winter temperatures and dust storm frequencies for a 500 year record in China. *Parungo et al.* [1995] find the occurrence of strong dust events in China associated with the arrival of cold fronts from Siberia at the Gobi desert. Strong winds associated with a cold front raise dust, which is then transported eastward over China to the North Pacific. In Plate 4, we show maps of correlation coefficients between dust concentration at Beijing and the climate parameters sea level pressure, precipitation, and surface temperature for GCM experiment A. In this region, no significant correlation can be found between precipitation and dust concentrations (Plate 4b). The pressure pattern which is correlated with high dust transport to Beijing (Plate 4a) shows high pressure over West Siberia, which favors an anticyclonic flow of arctic air into Northern Asia. This is reflected by negative correlation of Beijing dust concentration with temperatures over Siberia (Plate 4c). Table 5 shows the correlation coefficients for the individual seasons between the dust concentration at Beijing and the sea level pressure differences between the locations (50°N; 110°W) and (75°N; 60°E), the precipitation deficit in the area (30°N-50°N ; 90°E-110°E) and the surface temperature in the area (50°N- 60°N; 50°E -100°E) for experiments A and B. In the case of Chinese dust, springtime correlations between dust concentration and the pressure difference along with surface temperature are weaker for the fixed source experiment (B) than for variable sources (A). For fixed sources (no figure), wash-out by precipitation seems to be a controlling factor for dust concentration at Beijing, in contrast to the results for variable sources (Plate 4b). The different correlation at Beijing between the model experiments with fixed and variable sources indicate that the variability in dust sources caused by specific pressure patterns is a major influence on the interannual variability of Chinese dust. Presumably, these pressure patterns are associated with variations in surface wind speed, which modulates the surface dust emission. This is in contrast to the North Atlantic and Mediterranean dust, where variations in transport are the predominant cause of dust variability.

4. Conclusions

Dust was included as a dynamic tracer in a current version of the GISS GCM to explore the dependency of dust variability upon climate parameters such as precipitation and pressure patterns. The GCM integrations were carried out using fixed climatological sea surface temperatures. Even though there were no year-to-year changes in the SSTs, the interannual variability of dust concentration in the model was high. Comparison of dust variability from experiments with fixed monthly dust sources and dust sources that were calculated on-line with GCM precipitation and wind speeds show that for regions like the Mediterranean and North Atlantic, variability of dust transport rather than variability of source strength contributes most to the interannual variability of dust concentration. In other regions, like the Arabian Sea, the tropical North Atlantic, and Antarctica, a large fraction of dust variability in the model is attributable to variability in dust sources. Long-term observations that are intended to investigate trends in dust source strengths caused by either changes in climatic conditions or human impact should be carried out in regions with a lower contribution of transport variability to interannual dust concentration variations.

For specific regions the correlation between interannual changes in dust concentration and climate parameters such as sea level pressure and precipitation was also investigated. Even if the GCM cannot resolve small-scale dust storm systems (which play an important role in dust deflation and transport), it shows a realistic dependency between interannual variations in dust concentrations and circulation changes on a larger scale. This is encouraging and suggests that the GCM can be used to explain observed changes in the atmospheric dust load, as well as to predict changes in the dust load as a consequence of changes in climatic conditions.

GCM experiments using prescribed SSTs are just a first step in using a global model to understand the controlling factors in the soil dust cycle. A next step will

be to couple the atmospheric GCM to a mixed-layer or else dynamical ocean model to investigate the relation of dust fluxes to climate modes. Ultimately, this dust parameterization will be used to investigate the radiative effect of dust upon climate along with the feedback of the climate perturbations upon dust concentration.

Acknowledgments. This work was supported by the National Science Foundation (grant ATM-94-22631). Partial support was given by the NASA Earth Observing Systems program (NASA grant NAG5-4052), and by the NOAA office of global programs (grant NA56GP0450). Soil dust ground observations were supplied by D. Savoie and J. Prospero, University of Miami, and N. Kubilay, Columbia University.

References

Bergametti, G., L. Gomes, E. Remoudaki, M. Desbois, D. Martin, and P. Buat-Menard, Present transport and deposition patterns of African dusts to the northwestern mediterranean, in *Paleoclimatology and Paleometeorology: Modern and Past Patterns of Global Atmospheric Transport*, edited by M. Leinen and M. Sarntheim, pp. 227–252, Kluwer Acad., Norwell, Mass., 1989.

Carlson, T. N., and J. M. Prospero, The large-scale movement of Saharan air outbreaks over the northern equatorial Atlantic, *J. Appl. Meterol.*, *11*, 283–297, 1972.

Coakley, J. A., and R. D. Cess, Response of the NCAR Community Climate Model to the radiative forcing by the naturally occurring tropospheric aerosol, *J. Atmos. Sci.*, *42*, 1677–1692, 1985.

d'Almeida, G., and L. Schütz, Number, mass, and volume distribution of mineral aerosol and soils of the Sahara, *J. Clim. Appl. Meteorol.*, *22*, 233–243, 1983.

DelGenio, A. D., M.-S. Yao, W. Kovari, and K. K.-W. Lo, A prognostic parameterization for global climate models, *J. Clim.*, *9*, 270–304, 1996.

Dentener, F. J., G. R. Carmichael, Y. Zhang, J. Lelieveld, and P. J. Crutzen, Role of mineral aerosol as reactive surface in the global troposphere, *J. Geophys. Res.*, *101*, 22,869–22,889, 1996.

Duce, R. A., Sources, distributions, and fluxes of mineral aerosols and their relationship to climate, in *Aerosol Forcing of Climate*, edited by R. Charlson and J. Heintzenberg, pp. 43–72, John Wiley, New York, 1995.

Gardner, W. R., Soil properties and efficient water use, in *Limitations to Efficient Water Use in Crop Production*, edited by H. M. Taylor, W. R. Jordan, and T. R. Sinclair, Am. Soc. of Agron., 1983.

Genthon, C., Simulations of desert dust and sea salt aerosols in Antarctica with a general circulation model of the atmosphere, *Tellus, Ser. B*, *44*, 371–389, 1992.

Gillette, D., A wind tunnel simulation of the erosion of soil: Effect of soil texture, sandblasting, wind speed, and soil consolidation on dust production, *Atmos. Environ.*, *12*, 1735–1743, 1978.

Goudie, A. S., and N. J. Middelton, The changing frequency of dust storms through time, *Clim. Change*, *20*, 197–225, 1992.

Hansen, J. E., G. L. Russell, D. Rind, P. Stone, A. Lacis, S. Lebedeff, R. Ruedy, and L. Travis, Efficient three–dimensional global models for climate studies: Models I and II, *Mon. Weather Rev.*, *111*, 609–662, 1983.

Hansen, J., et al., Forcings and chaos in interannual to decadal climate change, *J. Geophys. Res.*, *102*, 25,679–25,720, 1997.

Herman, J. R., P. K. Bhartia, O. Torres, C. Hsu, C. Seftor, and E. Celarier, Global distribution of UV-absorbing aerosols from Nimbus 7/TOMS data, *J. Geophys. Res.*, *102*, 16,911–16,922, 1997.

Horel, J. D., A rotated principal component analysis of the interannual variability of the northern hemisphere 500 mb height field, *Mon. Weather Rev.*, *109*, 2080–2092, 1981.

Hurrell, J. W., Decadal trends in the North Atlantic Oscillation: Regional temperatures and precipitation, *Science*, *269*, 676–679, 1995.

Joussaume, S., Three-dimensional simulations of the atmospheric cycle of desert dust particles using a general circulation model, *J. Geophys. Res.*, *95*, 1909–1941, 1990.

Kubilay, N., and A. C. Saydam, Trace elements in atmospheric particulates over the eastern Mediterranean: Concentrations, sources, and temporal variability, *Atmos. Environ.*, *29*, 2289–2300, 1995.

Kutzbach, J., Empirical eigenvectors of sea level pressure, surface temperature, and precipitation complexes over North America, *J. Clim. Appl. Meteorol.*, *6*, 791–802, 1967.

Lacis, A. A., and M. I. Mishchenko, Climate forcing, climate sensitivity, and climate response: A radiative modeling perspective on atmospheric aerosols, in *Aerosol Forcing of Climate*, edited by R. Charlson and J. Heintzenberg, pp. 11–42, John Wiley, New York, 1995.

Lau, N.-C., and M. J. Nath, The role of the 'atmospheric bridge' in linking tropical Pacific ENSO events to extratropical SST anomalies, *J. Clim.*, *9*, 2036–2057, 1996.

Littmann, T., Dust storm frequency in Asia: Climatic control and variability, *Int. J. Climatol.*, *11*, 393–412, 1991.

Marticorena, B., and G. Bergametti, Two-year simulations of seasonal and interannual changes of the Saharan dust emissions, *Geophys. Res. Lett.*, *23*, 1921–1924, 1996.

Matthews, E., Global vegetation and land use: New high–resolution databases for climate studies, *J. Clim. Appl. Meteorol.*, *22*, 474–487, 1983.

Middelton, N., *World Atlas of Desertification*, Edward Arnold, London, 1992.

Miller, R. L., and X.-J. Jiang, Surface energy fluxes and coupled variability in the tropics of a coupled general circulation model, *J. Clim.*, *9*, 1599–1620, 1996.

Miller, R. L., and I. Tegen, Climate response to mineral dust aerosol, *J. Clim.*, in press, 1998.

Moulin, C., C. E. Lambert, F. Dulac, and U. Dayan, Control of atmospheric export of dust from North Africa by the North Atlantic Oscillation, *Nature, 387*, 691–694, 1997a.

Moulin, C., F. Guillard, F. Dulac, and C. E. Lambert, Long-term daily monitoring of Saharan dust load over ocean using Meteosat ISCCP-B2 data, 1, Methodology and preliminary results for 1983–1994 in the Mediterranean, *J. Geophys. Res., 102*, 16,947–16,958, 1997b.

North, G. R., T. L. Bell, and R. F. Calahan, Sampling errors in the estimation of empirical orthogonal functions, *Mon. Weather Rev., 110*, 699–706, 1982.

Parungo, F., et al., Asian dust storms and their effects on radiation and climate, *Tech. Rep. STC 2906*, Natl. Oceanic and Atmos. Admin., Silver Spring, Md., 1995.

Prospero, J. M., and R. T. Nees, Impact of the North African drought and El Niño on mineral dust in the Barbados trade winds, *Nature, 320*, 735–738, 1986.

Rao, C. R. N., L. L. Stowe, E. P. McClain, J. Sapper, and M. P. McCormick, Development and application of aerosol remote sensing with AVHRR data from the NOAA satellites, in *Aerosols and Climate*, edited by P. V. Hobbs, A. Deepak, Hampton, Va., 1988.

Schütz, L., R. Jaenicke, and H. Pietrek, Saharan dust transport over the North Atlantic Ocean, *Geol. Soc. Am. Spec. Pap. 186*, 87–100, 1981.

Stowe, L. L., A. M. Ignatov, and R. Singh, Development, validation, and potential enhancements to the second-generation operational aerosol product at the National Environmental Satellite, Data, and Information Service of the National Oceanic and Atmospheric Administration, *J. Geophys. Res., 102*, 16,923–16,934, 1997.

Tegen, I., and I. Fung, Modeling of mineral dust in the atmosphere: Sources, transport, and optical thickness, *J. Geophys. Res., 99*, 22,897–22,914, 1994.

Tegen, I., and I. Fung, Contribution to the mineral aerosol load from land surface modification, *J. Geophys. Res., 100*, 18,707–18,726, 1995.

Tegen, I., A. Lacis, and I. Fung, The influence of mineral aerosol from disturbed soils on the global radiation budget, *Nature, 380*, 419–422, 1996.

Tucker, C. J., H. E. Dregne, and W. W. Newcomb, Expansion and contraction of the Sahara desert from 1980 to 1990, *Science, 253*, 299–301, 1991.

Webb, R., C. Rosenzweig, and E. R. Levine, A global data set of particle size properties, *NASA Tech. Rep. TM-4286*, 33 pp., 1991.

Wefers, M., and R. Jaenicke, Global 3D distribution of desert aerosols from a numerical simulation, in *Proceedings 3rd International Aerosol Conference, Kyoto, Japan*, edited by S. Masuda and K. Takakashi, pp. 1086–1089, 1990.

World Resources Institute, *World Resources 1992–1993*, edited by A. L. Hammond. Oxford Univ. Press, New York, 1992.

Zhang, D. H., Chinese dust storm chronology and preliminary analysis on meteorology and climatology, *Sci. China*, 278–288, 1984.

Zinn, H. P., and A. D. Kowalski, An efficient PBL model for global circulation models - Design and validation, *Boundary Layer Meteorol., 75*, 25–59, 1995.

Zobler, L., A world soil file for global climate modeling, *NASA Tech. Rep. TM-87802*, 32 pp., 1986.

R. Miller and I. Tegen, NASA Goddard Institute for Space Studies, 2880 Broadway, New York, NY 10025. (e-mail: itegen@giss.nasa.gov)

(Received November 15, 1997; revised June 17, 1998; accepted June 24, 1998.)